



Parametric optimization of selected auxetic structures

Maciej Zawistowski¹ · Arkadiusz Poteralski¹

Received: 7 February 2024 / Accepted: 8 April 2024
© The Author(s) 2024

Abstract

Auxetic materials exhibit an interesting, counterintuitive behavior—when subjected to uniaxial tension, they stretch laterally, and when uniaxially compressed, they shrink laterally. In contrast to conventional materials, in auxetics, the value of Poisson's ratio is negative. Behavior of auxetic materials is an effect of their internal structures. The auxetic effect depends mostly on the geometry of their internal unit cells and not on the properties of the bulk material. This paper presents the results of parametric optimization of selected two-dimensional auxetic unit cells with the aim to identify the geometrical parameters which exhibit the strongest influence on the value of Poisson's ratio in each unit cell, and to identify geometries which exhibit the strongest auxetic effect. The optimization was conducted through numerical simulation with the use of the finite element method in commercial software. Response surface optimization and multi-objective genetic algorithm (MOGA) were applied. Obtained candidate geometries were verified via additional FEM analyses and confirmed to have improved auxetic effect and reduced equivalent stress. 5×5 structures composed of reference and optimized geometries of analyzed unit cells were subjected to similar analyses and it was confirmed that the optimization of singular unit cells caused an improvement of auxetic effect and reduction in equivalent stress in regular structures composed of multiple unit cells.

Keywords Auxetic materials · Finite-element method · Numerical simulation · Parametric optimization

1 Introduction

Auxetic materials and structures behave contradictory to intuition—while uniaxially stretched, they both elongate and expand laterally and when uniaxially compressed, they both contract longitudinally and shrink laterally, as demonstrated in Fig. 1. In other words, in deformed auxetics, strains in specific directions share the same sign, positive during tension and negative during compression. This behavior is bound to the characteristic negative values of Poisson's ratio in auxetics and is the cause of their numerous, interesting potential applications.

While the theoretical range of Poisson's ratio from -1 to $+0.5$ based on the theory of isotropic linear elasticity was known since the nineteenth century, first observations of materials with negative Poisson's ratio were reported in

the first half of twentieth century by Love (1927) and Voigt (1928). They both noticed the peculiar behavior of pyrite crystals during their experiments. Love described an example of a cubic single-crystal pyrite as a material with negative Poisson's ratio equal to -0.14 . Almost 60 years later, in 1980s, numerous researchers tried and managed to successfully manufacture a synthetic foam with negative Poisson's ratio. Bhullar described those stages in more detail in his review (Bhullar 2015). Materials with negative Poisson's ratio are known as auxetics since 1991, when the term was coined by Evans (1991), derived from the Greek *αὐξητικός* (transliteration: *auxetikos*), meaning “that which tends to increase”.

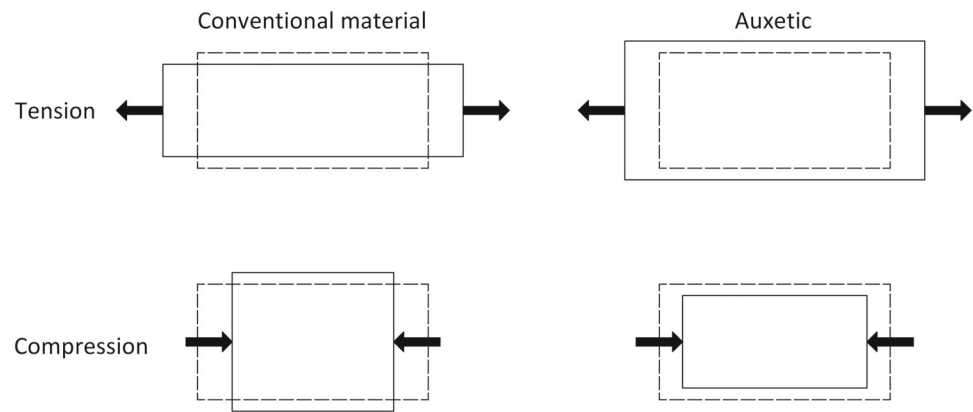
Specific behavior of auxetics is an effect of their internal structures. These structures consist of characteristic geometries, which when subjected to mechanical loading behave similarly to linkage mechanisms. The scale of auxetics' internal structures differs based on application, from macro- through micro- to nanoscale and molecular-level structures. Regardless of scale, in patterned structures, the auxetic effect depends mostly on the geometry of their unit cells (Lim 2015; Elipe and Lantada 2012). It is possible to obtain an auxetic by

✉ Maciej Zawistowski
maciej.zawistowski@polsl.pl

Arkadiusz Poteralski
arkadiusz.poteralski@polsl.pl

¹ Department of Computational Mechanics and Engineering,
Faculty of Mechanical Engineering, Silesian University of
Technology, Konarskiego 18A, 44-100 Gliwice, Poland

Fig. 1 Deformation during uniaxial loading of conventional materials and auxetics; dashed line—contour prior to loading, solid line—contour after loading



shaping a conventional material into a specific auxetic structure. Material obtained in this way is considered auxetic, even though the bulk material is conventional (Evans, Alderson 2000). Due to their unique properties, auxetic materials are considered smart materials. Due to the nature of their periodic structure, multiscale modeling is often applied in research of auxetics to analyze the behavior of elements made from auxetic structures, which are then treated as homogenous materials and have properties based on the results of analysis of a RVE (representative volume element) of the proper structure of the auxetic material. Simulations are mostly performed based on specific unit cells, which are the basic component of auxetic structures (Meena, Singamneni 2019; Wang et al. 2019).

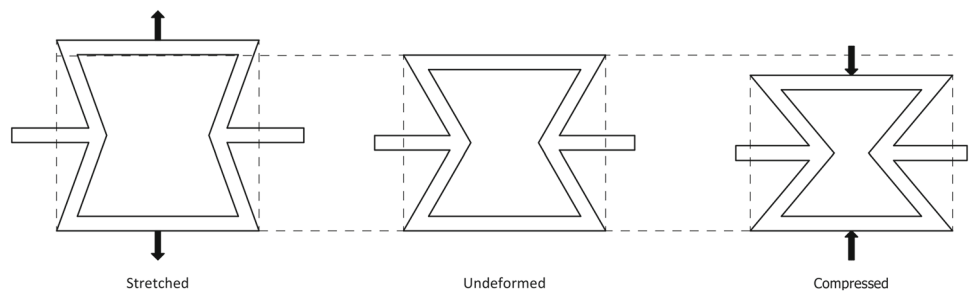
Auxetic structures are based on numerous deformation mechanisms, out of which the most common are the re-entrant mechanism, rotating unit mechanism and chiral mechanism (Cho et al. 2019). Re-entrant auxetic structures consist of thin ribs linked by hinges. Re-entrant unit cells include combinations of acute and reflex internal angles, which cause the structure to unfold outward in both directions during uniaxial stretching and to progressively fold inwards in both directions during uniaxial compression. Deformation pattern of exemplary re-entrant structure is demonstrated in Fig. 2. Rotating unit structures consist of regular rigid unit cells of one or few types of geometries which are connected to neighboring cells only by their corners. Application of force causes the unit cells to rotate, while remaining connected to each other by their corners, which results in a distinct change of pattern formed by the unit cells, and, in an auxetic deformation of the structure. Chiral structures, most commonly, consist of arrangements of unit circles with tangent straight ribs, which connect neighboring circles. Chiral structures are named based on the number of ribs protruding from a single circle in a unit cell, e.g., in trichiral structures, a single circle is connected to its neighbors by three ribs and in tetrachiral structures by four.

Unusual behavior of auxetics inspired researchers to think of many interesting potential applications (Evans and Alderson 2000). An intriguing example is a bullet composed of conventional and auxetic components, so that its overall Poisson's ratio would be equal to zero, which would significantly reduce the loss of bullet's kinetic energy due to friction during its movement down the barrel. Auxetics' deformation pattern causes them to also have increased indentation resistance and shock-absorption properties, which might be utilized in personal protective equipment, such as helmets and bullet-proof vests. Another interesting example of utilizing the auxetic effect is the concept of auxetic nail (Ren et al. 2018) which, in comparison to conventional nails, would be easier to push in, due to lateral contraction during compression, and harder to pull out, due to lateral expansion caused by tension. Auxetic materials can also find numerous applications in more concrete load-bearing applications, as indicated by Momoh et al. (2024) in their review of auxetics applications in cementitious composites. Auxetic geometries can be utilized in civil and structural engineering applications as structural load-bearing elements with increased impact energy absorption as well as in functional smart filtration systems.

Since the extent of auxetic effect is dependent mostly on geometry of the structure's unit cell, properties of the auxetic structure can be adjusted during the design phase to fulfill the desired requirements. Research papers which propose new types of auxetic structures, or new applications of structures that are already well known, often include a portion devoted to optimization of the considered auxetic structure geometry. Novak et al. (2022) proposed a novel 3D graded axisymmetric chiral auxetic structure, which they optimized by parametrizing thicknesses of 9 separate struts and managed to obtain a very significant increase in structure's stiffness. Other examples of optimization of auxetic structures with functional goals include (Behinfar and Nourani 2024; Bruggi et al. 2016; Gao et al. 2023; Gohar et al. 2021); ; .

One of the most notable fields of auxetic materials application is shock absorption, as such strain energy of auxetic

Fig. 2 Deformation pattern of auxetic hex re-entrant unit cell



structures and maximizing their ability to absorb impact energy is one of the most popular optimization goals. Tan et al. (2021) performed multi-objective optimization of an auxetic hierarchical honeycomb crash box and compared its crushing performance with an aluminum foam-filled crash box and a traditional crash box. The results showed that the auxetic crash boxes presented the strongest energy dissipation capacity, and that the optimization resulted in increase of specific energy absorption and mean crushing force compared to the initial geometry. Wang et al. (2020) performed a similar analysis of crashworthiness for a novel crash box with core of auxetic hex re-entrant structure with collaborative optimization design.

A separate area of research interest that is currently extensively explored is the use of computational intelligence, such as machine learning, for automated optimization of auxetic structures. Wang et al. (2023) proposed the use of machine learning to accelerate the design of auxetic structures. The structures they obtained exhibited very strong auxetic effect (-1.35 up to -1.50), which was later confirmed experimentally, but the complex zig-zag geometry of the structure limited the effective strain to which it could be subjected without permanent deformation to 2.526%. Meier et al. (2024) proposed an automated optimization approach in obtaining auxetic and isotropic metamaterials in counterintuitive design spaces. They arranged 8 distinct neither isotropic nor auxetic unit cells together in a $5 \times 5 \times 5$ cubic symmetric lattice structure with controlled automated modeling approach. They managed to obtain a structure which exhibited 0.01 value of Poisson ratio by combining component structures which were not auxetic, to obtain auxetic effect inside the cubic structure which allowed them to obtain almost zero-value lateral strain. Similar work with very different approach was published by Long et al. (2016), where they considered a composite material composed of auxetic phase and conventional phase. They considered homogenous materials with arbitrarily set values of the Poisson's ratio and Young's modulus and used computational intelligence method to obtain a cubic structure of composite material with increased Young's modulus in regard to both component phases.

This paper presents the results of parametric optimization of selected two-dimensional auxetic unit cells with the aim to maximize the auxetic effect while maintaining a safe level of mechanical stress. FEM simulation and optimization were conducted with the use of Ansys[®] Academic Research Workbench Mechanical 2023 R1 software. Two types of two-dimensional unit cells were analyzed, the 4-vertice star unit cell and the elongated chevron unit cell. 4-vertice star can be considered a part of a larger “family” of unit cells composed of a cross, in which orthogonal arms are connected to each other with a compliant geometry, in this case, the star arm with angle α , other notable examples include the tetra petal unit cell and its variations, like ones considered by Wang et al. (2019). Elongated chevron unit cell is based on the structure often referred to as the “US Patent Pyramid” (Ma 2008, US7910193B2), adjusted to enlarge the contact surfaces between neighboring unit cells and prevent stress concentration. These two unit cells have been selected for optimization as representatives of two different groups of auxetic unit cells. The 4-vertice star is isotropic, while elongated chevron is strongly anisotropic. By investigating the two of them together, it was possible to verify the effectiveness of presented approach on examples of two different specific auxetic unit cells, which represent two different groups of auxetic unit cells.

The novelty of this paper lies in multi-objective optimization and comparison of two very different type of auxetic geometries, with the goal to maximize the auxetic effect of the structures and reduce their equivalent stress. The results can be used in further research of multiphase materials with auxetic phase. The presented method allows to obtain auxetic geometries based on known unit cells with custom-tailored properties, which will allow to design multiphase materials with material properties grounded in separate simulation results, instead of arbitrarily imposed by the authors.

2 Methodology and analyzed unit cells

Poisson's ratio is the most important measure of auxetic effect. It gives the proportion of transversal strain to axial

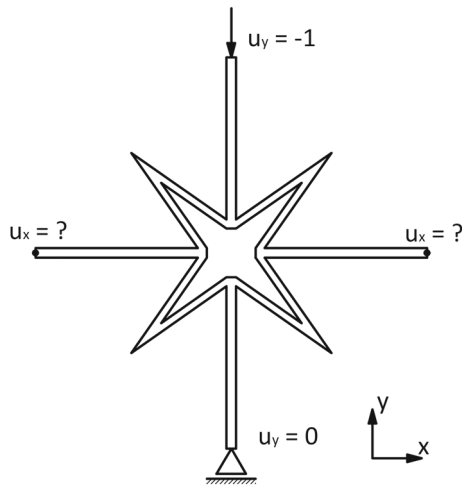


Fig. 3 4-vertex star unit cell with marked displacement boundary conditions

strain during uniaxial loading:

$$\nu = -\frac{\varepsilon_T}{\varepsilon_A} \quad (2.1)$$

where ν is the Poisson's ratio, ε_T is the strain in transversal direction and ε_A is the strain in axial direction (direction of loading). In case of auxetic structures analysis, the structure's effective Poisson's ratio is more commonly used than the material's general Poisson's ratio. In case of effective Poisson's ratio, only effective strains of the analyzed structure are taken into consideration:

$$\nu_{\text{eff}} = -\frac{\varepsilon_{\text{Teff}}}{\varepsilon_{\text{Aeff}}} \quad (2.2)$$

Effective strains are calculated based on displacements of the structure's most external edges, those which would be the contact surfaces with neighboring unit cells in case of periodic structures. For example, in case of 4-vertex star

unit cell shown in Figs. 3 and 4, effective strains would be calculated based only on displacements of the four external edges of the star orthogonal arms. For a 4-vertex star unit cell, loaded as shown in Fig. 3 and with dimensions as shown in Fig. 4, the effective strains are calculated as follows:

$$\varepsilon_{\text{Aeff}} = \frac{u_y}{2b} \quad (2.3)$$

and:

$$\varepsilon_{\text{Teff}} = \frac{u_x}{2b} \quad (2.4)$$

where u_y is the sum of displacements in the y direction of the cell's external top and bottom edges, and u_x is the sum of displacements in the x direction of the cell's external left and right edges, b is the cell's arm length, equal to half of its total width or length in undeformed state.

Figure 3 demonstrates the displacement boundary conditions assumed during FEM analysis of considered unit cells: rolling support of the bottom edge and vertical displacement of the top edge by the magnitude of -1 mm. In case of all considered structures, finite elements with quadratic shape function and global element size equal to 0.25 mm were applied, so that there were at least three finite elements at structure's width. The simulation was conducted with the use of 2-dimensional finite elements with quadratic shape function. QUAD-dominant method was used for meshing, the mesh consisted mostly of uniform quadrilateral elements with some triangular elements in places where algorithm failed to obtain a uniform quadrilateral mesh. Material properties of ABS polymer were assumed: Young's modulus E equal to 1.628 GPa and Poisson's ratio ν equal to 0.4089 .

The boundary conditions for 5×5 structures were similar to the ones for singular unit cells—a roller support was applied to the bottom edges of unit cells in the bottom row and vertical displacement by the magnitude of 2 mm was applied

Fig. 4 Analyzed unit cells with geometric parameters: 4-vertex star (left) and elongated chevron (right)

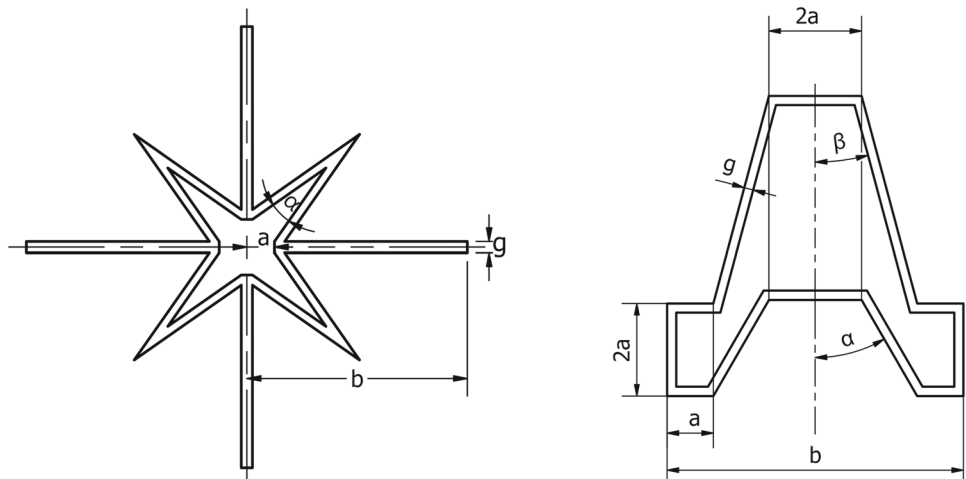


Table 1 Parameters of 4-vertice star unit cell

Parameter	Reference value	Optimization range
α	20°	16°–24°
a	3.75 mm	3–4.5 mm
b	24 mm	20–28 mm
g	1 mm	– (constant 1 mm)

Table 2 Parameters of elongated chevron unit cell

Parameter	Reference value	Optimization range
α	30°	24°–36°
β	15°	12°–18°
a	5 mm	4–6 mm
b	32 mm	25.6–38.4 mm
g	1 mm	– (constant 1 mm)

to the top edges of the unit cells in the top row. Horizontal displacement of all external edges, that would be connected to the next unit cells, of unit cells in the extreme right and left vertical rows were measured and averaged for the determination of the effective Poisson's ratio. Uniform mesh of finite elements of the same type and size as in singular unit cells' analyses was applied.

First, analyses and optimization were performed on singular unit cells and later additional analyses were performed on 5×5 structures composed of 25 unit cells, to verify the final optimization results in case of each analyzed geometry type. Two types of auxetic unit cells were analyzed and optimized: 4-vertice star and elongated chevron. Analyzed unit cells are shown in Fig. 4. Reference values and optimization range of geometric parameters for each unit cell are given in Tables 1 and 2.

ANSYS software built-in response surface optimization tool was utilized. Multi-objective genetic algorithm (MOGA) method was applied. The utilized built-in optimization tool is based on response surface approximation. First, a series of FEM analyses is conducted for the specified set of input parameters. Then, based on obtained results, the response surface is generated. The response surface is then searched for the best results with the multi-objective genetic algorithm. Finally, the obtained set of candidates (proposed results) is used as input data in FEM analyses to verify whether the approximation was precise, and whether the approximation results are compliant with results of actual FEM simulation. Multi-objective optimization was based on searching the Pareto frontier.

The primary goal of optimization was to maximize the auxetic effect, so to minimize the effective Poisson's ratio of

each unit cell. Secondary goal was to minimize the maximal and averaged equivalent stress (according to Huber–von Mises–Hencky hypothesis). Obtained candidates were verified via static structural simulation. Finally, the best candidates were selected. The best candidates are referred to as “Optimized”, while the reference geometries are referred to as “Reference”, in Figs. 5, 6, 7 and 8. The best candidates of optimized unit cells were then used in composition of 5×5 structure. Optimized structures were compared with reference ones. Objective function of optimization was formulated as follows:

$$\begin{aligned} v_{\text{eff}}(\alpha, \beta, a, b) &\Rightarrow \min, \\ \sigma_{\text{max}}(\alpha, \beta, a, b) &\Rightarrow \min, \\ \sigma_{\text{avg}}(\alpha, \beta, a, b) &\Rightarrow \min \end{aligned} \quad (2.5)$$

where σ_{max} is the maximal equivalent stress (Huber–von Mises–Hencky) observed in the unit cell, σ_{avg} is the averaged equivalent stress in the unit cell, and α, β, a, b are the cells' geometric parameters as specified in Tables 1 and 2 and Fig. 4. Additional constraints of maximal value were applied to the maximal and averaged stress output parameters.

3 Results

Optimization results are given in Tables 3 and 4, respectively for the 4-vertice star and the elongated chevron unit cells. Distributions of displacements and equivalent stress during uniaxial compression obtained by static structural FEM analysis are given in Figs. 5 and 6, and graphs visualizing the changes of input and output parameters during optimization are given in Figs. 9 and 10, respectively, for the 4-vertice star and the elongated chevron unit cells.

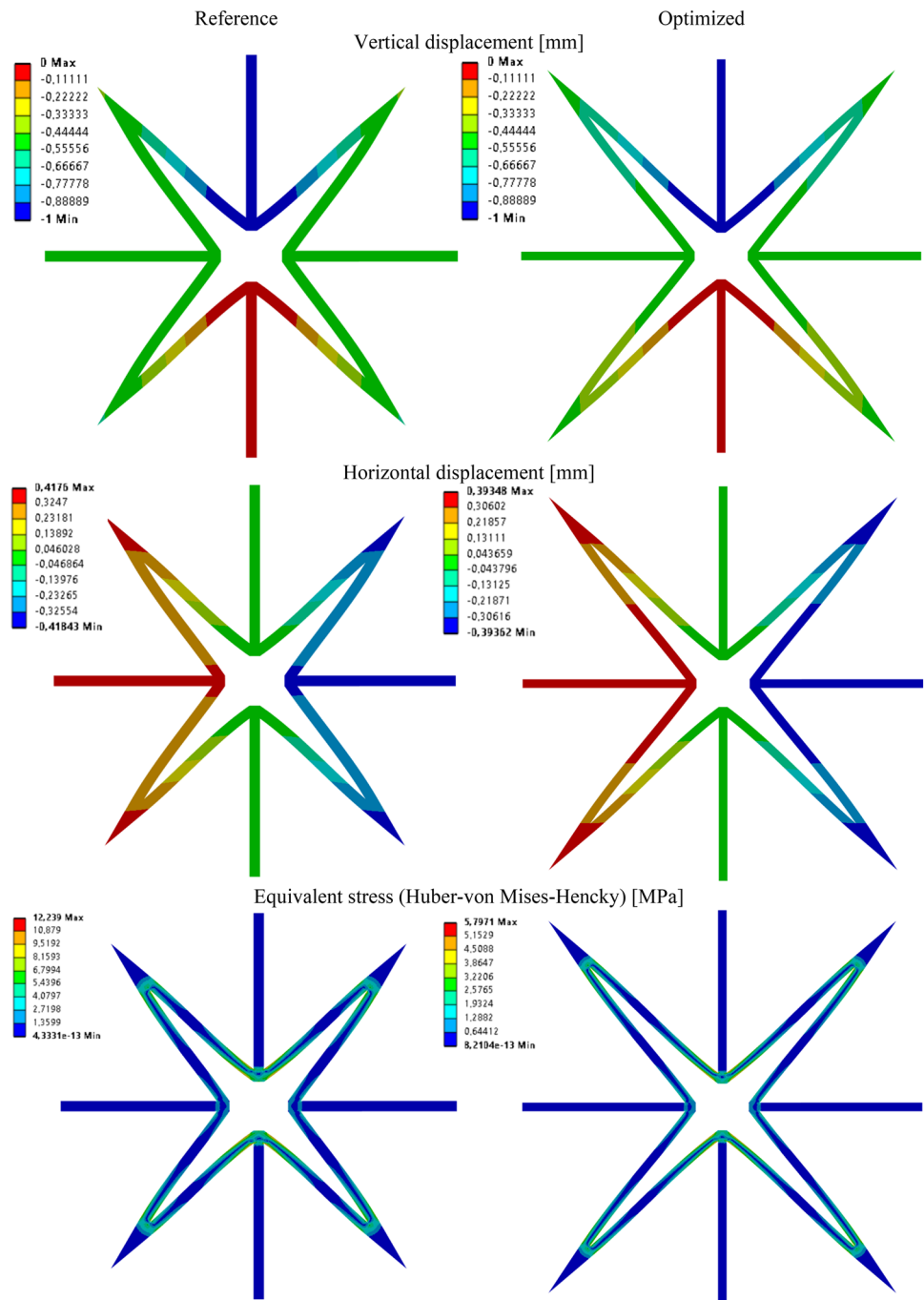
3.1 5×5 structures

Distributions of displacements and stress for 5×5 structures composed of reference and optimized unit cells are shown in Figs. 7 and 8, respectively, for the 4-vertice star and the elongated chevron structures. Comparison of reference and optimized structures' effective Poisson's ratio and stress is given in Tables 5 and 6, respectively, for the 4-vertice star and the elongated chevron structures.

4 Summary and conclusions

The aim of this study was to perform parametric optimization of selected auxetic unit cells with the aim to increase their auxetic effect and reduce equivalent stress. The effectiveness of optimization for the considered unit cells was compared and geometrical parameters with the highest influence on the auxetic effect were identified. The optimization results for

Fig. 5 Comparison of directional displacements and equivalent stress of reference and optimized 4-vertex star unit cell



singular unit cells were validated by conducting analyses of 5×5 structures composed out of the reference unit cells and optimized unit cells.

The conclusions are as follows:

1. Out of the analyzed structures the elongated chevron unit cell exhibited much stronger auxetic effect. It is bound to its distinctively anisotropic behavior, which needs to be taken into consideration while designing applications utilizing this type of structure. In case of 4-vertex star unit cell the effective Poisson's ratio remains in the range
2. In case of both unit cells, optimization significantly increased the auxetic effect and reduced equivalent stress. It is worth noting that the increase of auxetic effect was even greater in case of 5×5 structures composed of optimized unit cells.
3. Observing the plots of parameters change during the course of optimization allows to identify the geometric parameters' influence on structure's auxetic effect.

Fig. 6 Comparison of directional displacements and equivalent stress of reference and optimized elongated chevron unit cell

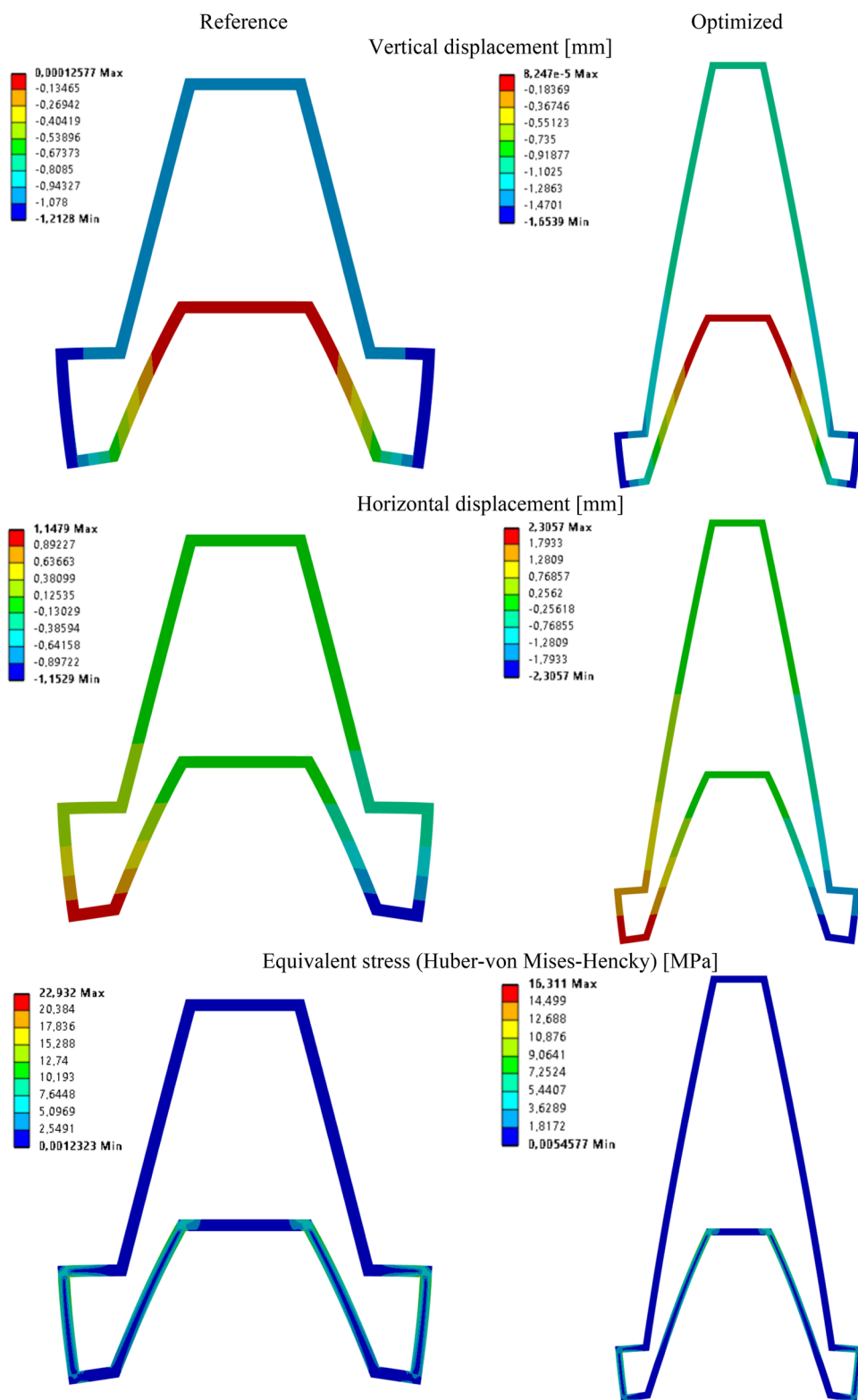
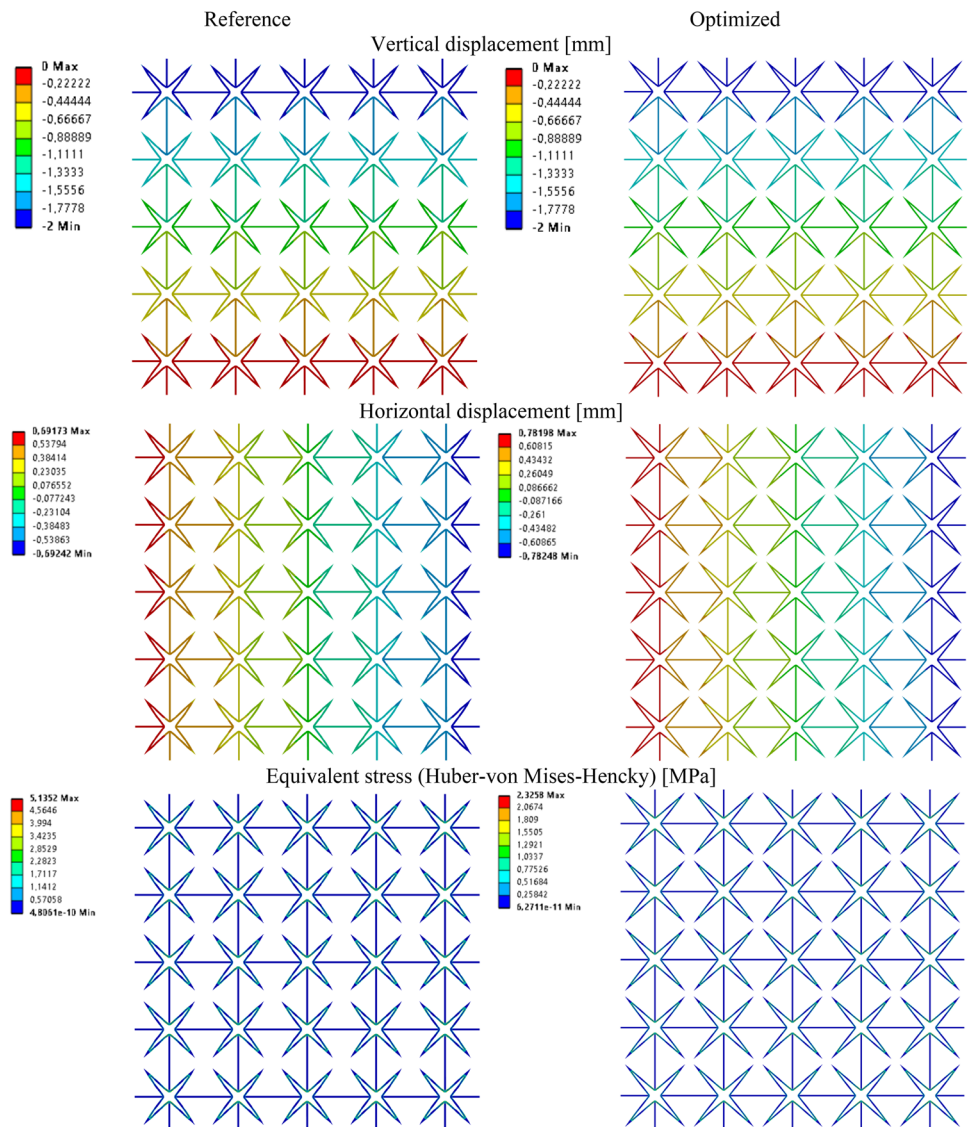


Fig. 7 Comparison of directional displacements and equivalent stress of reference and optimized 5×5 structures composed of 4-vertice star unit cells



In case of 4-vertice star unit cell, it increases with the increase of internal gap a and with the decrease of angle α . Chaotic changes of arm's length b during optimization suggest that this parameter does not have a strong influence on the magnitude of unit cell's effective Poisson's ratio. A similar observation was made in the previous study (Zawistowski and Poteralski 2023). In case of elongated chevron unit cell, the structure's auxetic effect increases with the increase of chevron's width b and the decrease of angles α and β , and dimension a .

- Effective Poisson's ratio of auxetic unit cells and structures composed out of them is dependent on the values and proportions of their geometric parameters. It is possible to effectively manipulate the magnitude of auxetic effect by changing the values of identified geometric parameters. The results of this work are also applicable

to design of micro-scale auxetic structures, by scaling down the unit cells dimensions.

- As the results show, it is possible to obtain singular auxetic unit cells, and by extension patterned auxetic structures composed out of this unit cells, with custom-tailored values of auxetic effect and reduced stress. This approach can be further utilized, allowing to effectively manipulate the material properties of considered structures, with the use of parametric optimization and known geometries of auxetic unit cells. This can prove useful in design of multiphase composite materials with auxetic phase, as when used together with multiscale modeling, it will allow to obtain component materials with specific material properties grounded in simulation results, instead of arbitrarily selected by the authors.

Fig. 8 Comparison of directional displacements and equivalent stress of reference and optimized 5×5 structures composed of elongated chevron unit cells

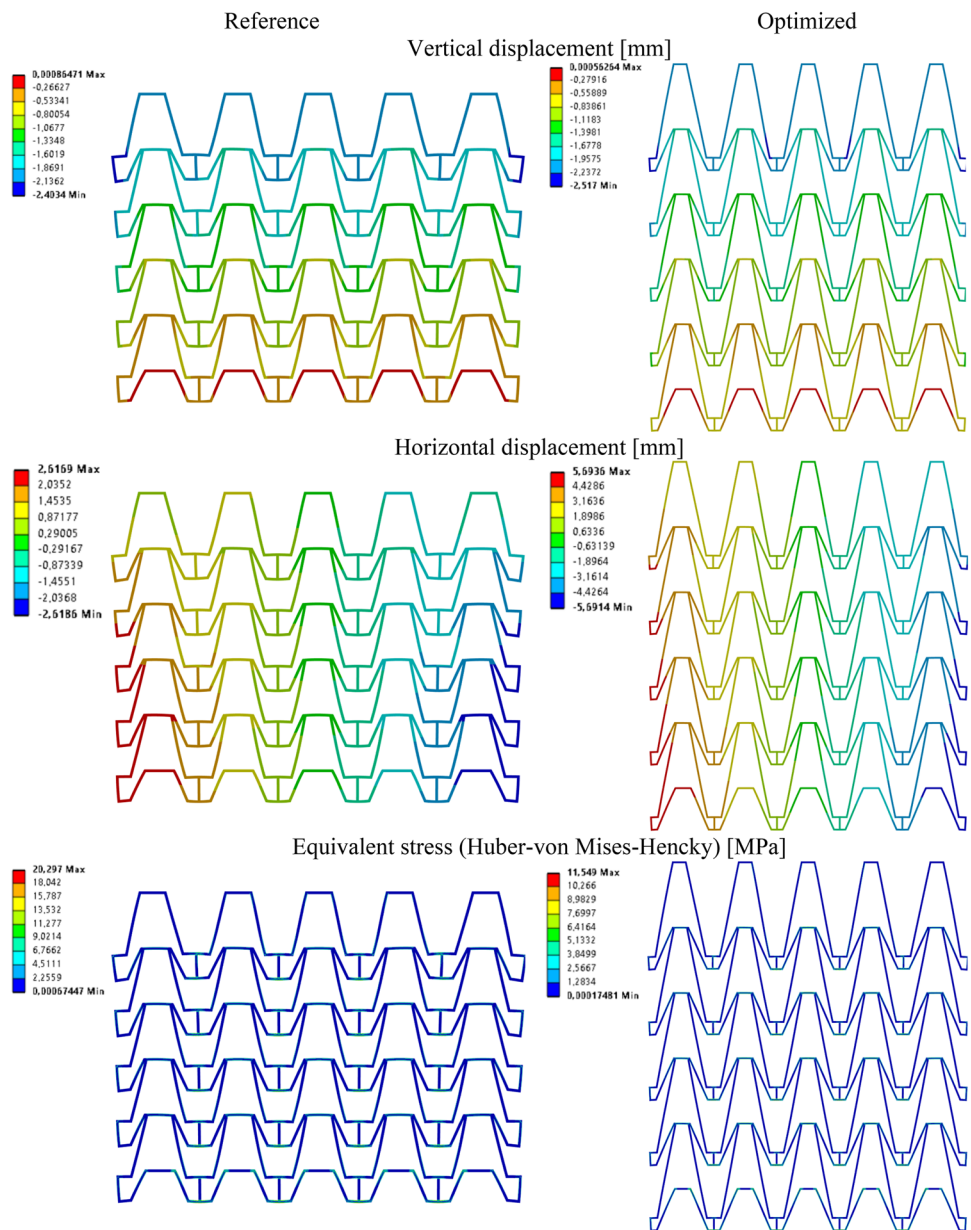


Table 3 Optimization results for the 4-vertice star unit cell

Parameter	Value		Optimization gain (%)
	Reference	Optimized	
α	20°	16.003°	− 19.99
a	3.75 mm	4.447 mm	18.59
b	20 mm	24.624 mm	23.12
g	1 mm	1 mm	–
Effective poisson’s ratio	− 0.657	− 0.781	18.87
Averaged equivalent stress	1.627 MPa	0.781 MPa	− 52.00
Maximal equivalent stress	12.276 MPa	5.797 MPa	− 52.78

Table 4 Optimization results for elongated chevron unit cell

Parameter	Value		Optimization gain (%)
	Reference	Optimized	
α	30°	26.306°	- 12.31
β	15°	12.011°	- 19.93
a	5 mm	4.006 mm	- 19.88
b	32 mm	38.362 mm	19.88
g	1 mm	1 mm	-
Effective poisson's ratio	- 1.252	- 4.201	235.54
Averaged equivalent stress	2.481 MPa	1.431 MPa	- 43.32
Maximal equivalent stress	22.934 MPa	16.311 MPa	- 28.88

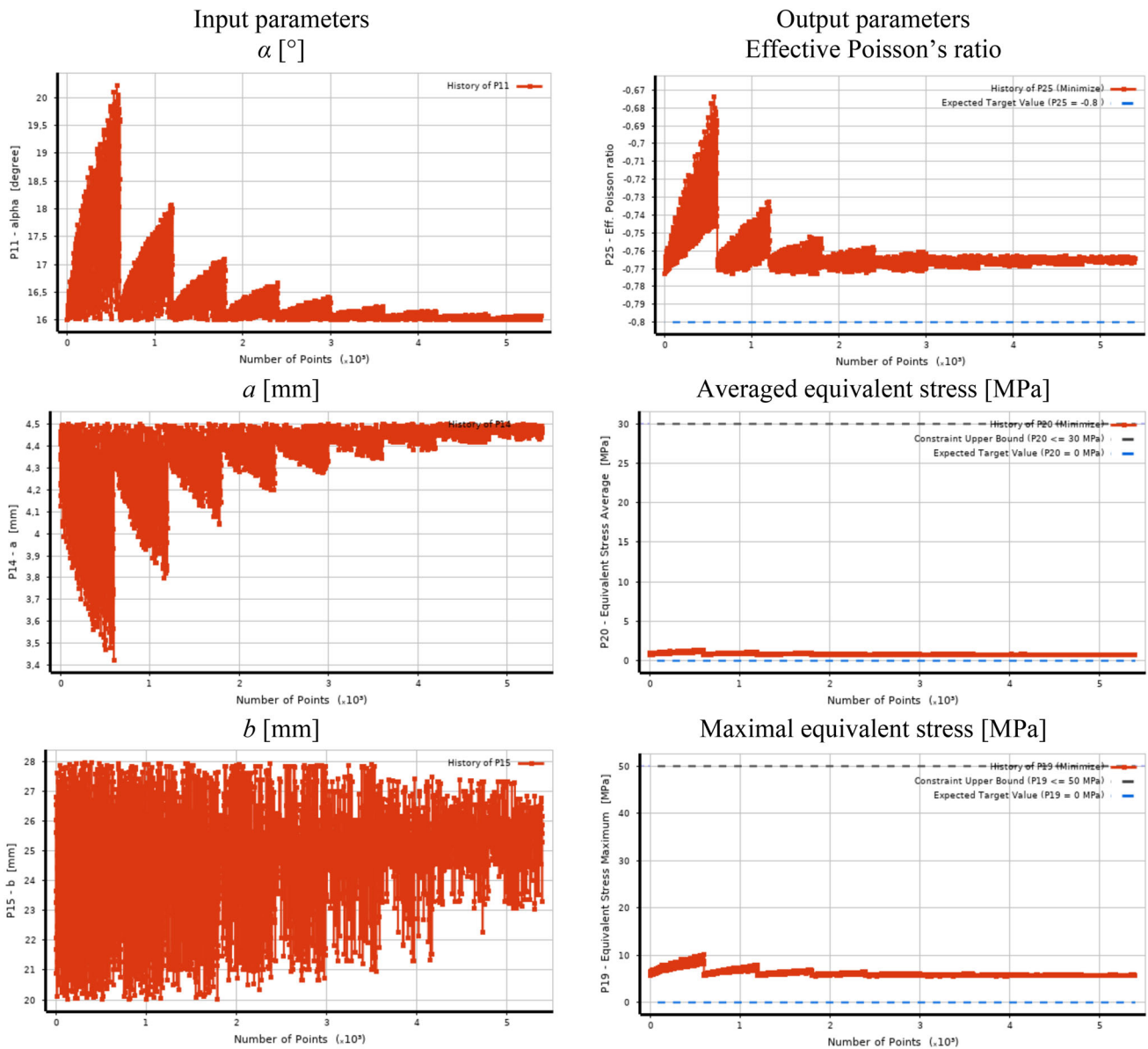


Fig. 9 Changes of 4-vertice star unit cell parameters during optimization

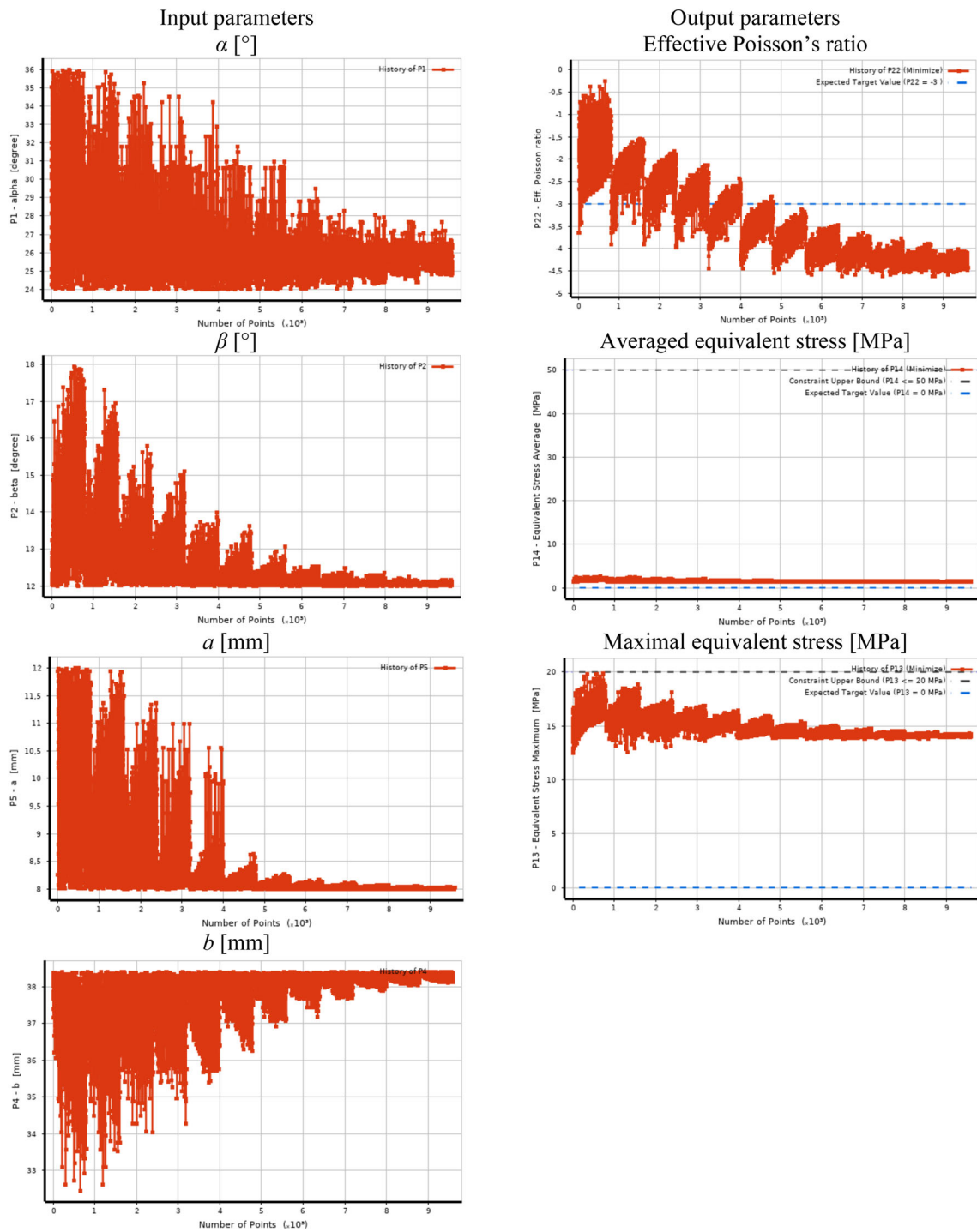


Fig. 10 Changes of elongated chevron unit cell parameters during optimization

Table 5 Optimization results for 5×5 structure composed of 4-vertex star unit cells

Parameter	Value		Optimization gain (%)
	Reference	Optimized	
Effective poisson's ratio	– 0.610	– 0.866	41.83
Averaged equivalent stress	0.631 MPa	0.300 MPa	– 52.46
Maximal equivalent stress	5.135 MPa	2.326 MPa	– 54.70

Table 6 Optimization results for 5×5 structure composed of elongated chevron unit cells

Parameter	Value		Optimization gain (%)
	Reference	Optimized	
Effective poisson's ratio	– 1.999	– 4.404	120.33
Averaged equivalent stress	1.795 MPa	0.891 MPa	– 50.36
Maximal equivalent stress	20.297 MPa	11.549 MPa	– 43.10

Acknowledgements The research was funded from the projects of Silesian University of Technology, Faculty of Mechanical Engineering.

Author contributions Conceptualization, A.P., M.Z.; formal analysis, M.Z., A.P.; simulations, M.Z., A.P.; verification, validation and testing, M.Z., A.P.; writing—review and editing, M.Z., A.P. All the authors have read and agreed to the published version of the manuscript.

Data availability No datasets were generated or analysed during the current study.

Declarations

Conflict of interest The authors declare no conflict of interest.

Open Access This article is licensed under a Creative Commons Attribution 4.0 International License, which permits use, sharing, adaptation, distribution and reproduction in any medium or format, as long as you give appropriate credit to the original author(s) and the source, provide a link to the Creative Commons licence, and indicate if changes were made. The images or other third party material in this article are included in the article's Creative Commons licence, unless indicated otherwise in a credit line to the material. If material is not included in the article's Creative Commons licence and your intended use is not permitted by statutory regulation or exceeds the permitted use, you will need to obtain permission directly from the copyright holder. To view a copy of this licence, visit <http://creativecommons.org/licenses/by/4.0/>.

References

- Behinfar P, Nourani A (2024) Analytical and numerical solution and multi-objective optimization of tetra-star-chiral auxetic stents. *Discov Appl Sci* 6:39
- Bhullar SK (2015) Three decades of auxetic polymers: a review. *E-Polymers* 15(4):205–215
- Bruggi M, Zega V, Corigliano A (2016) Optimization of auxetic structures for MEMS applications. In: 17th international conference on thermal, mechanical and multi-physics simulation and experiments in microelectronics and microsystems (EuroSimE)

- Cho H, Seo D, Kim DN (2019) Mechanics of auxetic materials. In: Schmauder S, Chen CS, Chawla K, Chawla N, Chen W, Kagawa Y (eds) *Handbook of mechanics of materials*. Springer, Singapore
- Elipe JCA, Lantada AD (2012) Comparative study of auxetic geometries by means of computer-aided design and engineering. *Smart Mater Struct* 21:10
- Evans KE (1991) Auxetic polymers: a new range of materials. *Endeavour* 15(4):170–174
- Evans KE, Alderson A (2000) Auxetic materials: functional materials and structures from lateral thinking! *Adv Mater* 12:9
- Gao Q et al (2023) Enhancing the output performance of energy harvesters using hierarchical auxetic structure and optimization techniques. *IEEE Trans Ind Electron* 2023:1
- Gohar S, Hussain G, Ilyas M, Ali A (2021) Performance of 3D printed topologically optimized novel auxetic structures under compressive loading: experimental and FE analyses. *J Mark Res* 2021(15):394–408
- Lim TC (2015) *Auxetic materials and structures*. Springer, Singapore
- Long K, Du X, Xu S, Xie YM (2016) Maximizing the effective young's modulus of a composite material by exploiting the Poisson effect. *Compos Struct* 153:596–600
- Love AE (1927) *A treatise on the mathematical theory of elasticity*, 4th edn. Cambridge university press, Dover, New York, p 163
- Ma ZH (2008) Three-dimensional auxetic structures and applications thereof (United States of America Patent no. US7910193B2)
- Meena K, Singamneni S (2019) A new auxetic structure with significantly reduced stress concentration effects. *Mater Des* 173:107779
- Meier T et al (2024) Obtaining auxetic and isotropic metamaterials in counterintuitive design spaces: an automated optimization approach and experimental characterization. *Comput Mater* 10:3
- Momoh EO, Jayasinghe A, Hajsadeghi M, Vinai R, Evans KE, Kripakaran P, Orr J (2024) A state-of-the-art review on the application of auxetic materials in cementitious composites. *Thin Walled Struct* 196:111447
- Novak N, Nowak M, Vesenjak M, Ren Z (2022) Structural optimization of the novel 3D graded axisymmetric chiral auxetic structure. *Phys Status Solidi B* 259:2200409
- Ren X et al (2018) Auxetic nail: design and experimental study. *Compos Struct* 184:288–298
- Tan H, He Z, Li E, Cheng A, Chen T, Tan X, Li Q, Xu B (2021) Crashworthiness design and multi-objective optimization of a novel auxetic hierarchical honeycomb crash box. *Struct Multidiscip Optim* 2021(64):2009–2024
- Voigt W (1928) *Lehrbuch der Kristallphysik* Teubner (in German)
- Wang ZP et al (2019) Systematic design of tetra-petals auxetic structures with stiffness constraint. *Mater Des* 170:107669

- Wang T, Li Z, Wang L, Hulbert GH (2020) Crashworthiness analysis and collaborative optimization design for a novel crash-box with re-entrant auxetic core. *Struct Multidiscip Optim* 62:2167–2179
- Wang M, Sun S, Zhang TY (2023) Machine learning accelerated design of auxetic structures. *Mater Des* 234:112334
- Zawistowski M, Poteralski A (2023) Analysis of geometric parameters influence on lateral strain of selected auxetic elementary cells. *Metod Komput* 2023:113–116 (**in Polish**)

Publisher's Note Springer Nature remains neutral with regard to jurisdictional claims in published maps and institutional affiliations.